THE ASTROPHYSICAL JOURNAL, 492:342–351, 1998 January 1

HIGH-SPEED OPTICAL PHOTOMETRY OF THE ULTRACOMPACT X-RAY BINARY 4U 1626−67

DEEPTO CHAKRABARTY[1,2]
Center for Space Research, Massachusetts Institute of Technology, Cambridge, MA 02139; deepto@space.mit.edu
Received 1997 June 3; accepted 1997 August 13

ABSTRACT

Rapid *UBVRI* photometry of the ultracompact low-mass X-ray binary (LMXB) pulsar 4U 1626−67/KZ TrA has detected 130.4 mHz (7.67 s) optical pulsations in all five bands. The optical pulsations, at the same frequency as the X-ray pulsations caused by rotation of the highly magnetized accreting neutron star primary, can be understood as a reprocessing of the pulsed X-ray emission in the accretion disk. The optical pulsed fraction is roughly 6%, independent of wavelength, indicating that the optical emission is dominated by X-ray reprocessing.

A weaker (1.5%) sideband, downshifted 0.395(15) mHz from the main optical pulsation, is also present. This is consistent with a previously reported sideband downshifted 0.4011(21) mHz from the main pulsation, corroborating the 42 minute binary period proposed by Middleditch et al. A 0.048 Hz optical quasi-periodic oscillation (QPO), corresponding to a previously reported X-ray feature, was also detected in some of the observations, with a fractional rms amplitude of 3%–5%. This is the first measurement of an optical QPO in an X-ray binary pulsar.

I discuss constraints on the nature of the mass donor and show that mass transfer via a radiatively driven wind is inconsistent with the optical data. I also review the basic theory of X-ray–heated accretion disks and show that such models provide a good fit to the optical photometry. If the effective X-ray albedo of LMXB accretion disks is as high as recently reported ($\eta_d \gtrsim 0.9$), then the optical data imply a distance of ~ 8 kpc and an X-ray luminosity of $\approx 10^{37}$ ergs s^{-1}.

Subject headings: accretion, accretion disks — binaries: close — pulsars: individual: 4U 1626−67 — stars: low-mass, brown dwarfs — stars: neutron

1. INTRODUCTION

The optical emission from low-mass X-ray binaries (LMXBs) is generally dominated by the reprocessing of X-rays in the accretion disk and/or the mass donor (see van Paradijs & McClintock 1995 for a review). The time history of the optical emission is thus a convolution of the X-ray intensity history with a function representing the spatial distribution of matter in the system. The most spectacular examples of this phenomenon are the optical novae accompanying soft X-ray transients, which can cause the optical counterpart to brighten by many magnitudes.

Of greater interest are those systems for which the X-ray intensity history is more regularly or sharply modulated. Many LMXBs show periodic optical variability as a result of orbitally modulated viewing of the X-ray–heated mass donor, providing constraints on the binary inclination and the distribution of reprocessing material in the system (see van Paradijs & McClintock 1995 and references therein). Quasi-periodic oscillations (QPOs) at various frequencies have been observed in both the X-ray and optical emission from the candidate black hole binary GX 339–4 (Motch, Ilovaisky, & Chevalier 1982; Motch et al. 1983; Imamura et al. 1990). Correlated X-ray and optical bursts have been observed from several systems, and both the time delay and the smearing of the optical burst profiles with respect to the X-ray bursts have been used to probe the location and distribution of matter near the neutron star (Lewin, van Paradijs, & Taam 1993). Coherent optical pulsations have been detected from the LMXB pulsars Her X-1 (Davidsen et al. 1972; Middleditch & Nelson 1981), 4U 1626−67 (Ilovaisky, Motch, & Chevalier 1978; Middleditch et al. 1981), and GX 1+4 (Jablonski et al. 1997), which likewise provide an important probe of the binary parameters and the distribution of reprocessing material in the system.

The LMXB 4U 1626−67/KZ TrA consists of a 7.66 s pulsar accreting from an extremely low mass companion in an ultracompact binary with a separation of <1 lt-s (Middleditch et al. 1981; Levine et al. 1988). The 7.66 s X-ray pulsations arise from anisotropic accretion of matter on the surface of a rotating, highly magnetized neutron star in which the spin and magnetic dipole axes are misaligned. The spin frequency of the pulsar evolves on short ($|\nu/\dot{\nu}| \approx$ 6000 yr) timescales because of accretion torques (Chakrabarty et al. 1997). The optical counterpart has a strong ultraviolet excess (McClintock et al. 1977), and optical pulsations are detected with the same frequency as the X-ray pulsations (Ilovaisky et al. 1978). The optical emission is understood to be primarily due to reprocessing of the incident X-ray flux by material in the accretion disk (Chester 1979; McClintock et al. 1980). The system shows strong, correlated X-ray/optical flares every ~ 1000 s that are of undetermined origin (Joss, Avni, & Rappaport 1978; McClintock et al. 1980; Li et al. 1980). A ~ 0.04 Hz QPO has been detected in the X-ray emission (Shinoda et al. 1990; Angelini et al. 1995), which probably arises through an interaction between the pulsar's magnetosphere and the inner edge of the accretion disk (Alpar & Shaham 1985; Lamb et al. 1985).

[1] NASA Compton GRO Postdoctoral Fellow.

[2] Visiting astronomer, Cerro Tololo Inter-American Observatory, National Optical Astronomy Observatories, operated by the Association of Universities for Research in Astronomy under contract to the National Science Foundation.

TABLE 1

LONG OBSERVATIONS OF 4U 1626 − 67

Run ID	Date	Start time (UT)	Duration (hr)	Filter	High-frequency Contaminant?[a]	Pulsations?
15U.....	1995 May 26	0408	2.0	*U*	No	Yes (strong detection)
17B	1995 May 26	0638	1.8	*B*	Yes	Yes (strong detection)
21I.....	1995 May 27	0018	1.7	*I*	No	No (clouds)
23R	1995 May 27	0308	1.9	*R*	No	Yes (strong detection)
25V2.....	1995 May 27	0604	0.6	*V*	Yes	No (clouds)
29U.....	1995 May 28	0001	0.7	*U*	Yes	No (clouds)
30U.....	1995 May 28	0046	1.0	*U*	Yes	Yes
32V	1995 May 28	0224	1.0	*V*	Yes	Yes
35U.....	1995 May 28	0709	1.0	*U*	Yes	Yes
36I.....	1995 May 28	0813	1.0	*I*	Yes	Yes (weak detection)

[a] Instrumental signals at harmonics of 1.75 Hz and 60 Hz.

High-sensitivity timing of the optical pulsations detected an additional weak, persistent pulsation in a lower frequency sideband of the "direct" (X-ray) pulse frequency (Middleditch et al. 1981). This sideband was attributed to X-ray reprocessing on the surface of the companion, meaning that the 0.4 mHz downshift is due to the different effective pulsar rotation rates observed in the companion frame owing to the binary orbit.[3] The observed frequency shift implies a 42 minute prograde orbit. X-ray timing measurements have repeatedly failed to detect periodic pulse arrival time delays or pulse frequency shifts due to a binary orbit, yielding an upper limit of $a_X \sin i \lesssim 10$ lt-ms for the projected radius of the neutron star orbit (Levine et al. 1988; Shinoda et al. 1990). For a 42 minute orbit, the X-ray timing limits imply a mass function $f_X(M) \leq 10^{-6}\ M_\odot$, one of the smallest known for any stellar binary.

This paper describes a program to confirm the persistent orbital sideband reported by Middleditch et al. (1981) and also provides the first detailed study of the optical wavelength dependence of X-ray reprocessing in this system. As part of this program, the first example of an optical QPO in an X-ray pulsar system was discovered. A preliminary account of this work has appeared previously in Chakrabarty (1996).

2. OBSERVATIONS

High-speed multicolor optical photometry of 4U 1626−67/KZ TrA was obtained during UT 1995 May 26–May 28 (MJD 49863–49865) with the 4 m Blanco telescope at the Cerro Tololo Inter-American Observatory (CTIO) in La Serena, Chile. The observations used the Automated Single Channel Aperture Photometer (ASCAP) and a dry ice–cooled Varian VPM-159A photomultiplier tube at the *f*/7.5 Ritchey-Chretien focus, along with the *UBVRI* filter set described by Graham (1982). The Varian phototube, which has an InGaAsP photocathode, is sensitive over a wide wavelength range, with a quantum efficiency of 15% at 4000 Å and 5% at 9000 Å. All the observations were made through a 6″.6 circular aperture. The data were recorded at 1 ms resolution and rebinned to 100 ms resolution for timing analysis. A log of the long timing observations of 4U 1626−67 is given in Table 1. Typical target and sky count rates are given in Table 2. The Graham (1982) photometric standard star E7-s was also observed at various airmasses on each night as a calibration source.

Timing stability was maintained using a Kinemetrics Truetime 468-DC GOES satellite synchronized clock. This clock was synchronized using NIST timing signals transmitted via the NOAA *Geostationary Operational Environmental Satellite 7* (*GOES West*), located in geostationary orbit at 135° west longitude (Beehler & Lombardi 1990). The signals were corrected for the 267 ms mean path delay from the NOAA ground station at Wallops Island, Virginia up to *GOES West* and down to the CTIO receiver (corresponding to a setting of 57 ms for the propagation delay switch on the clock). According to the manufacturer specifications, the clock in this configuration maintains absolute time accuracy within ±1.5 ms of UTC(NIST). However, an independent check of this accuracy (e.g., a cross-check with a Global Positioning System timing signal or optical pulse timing of a well-established astrophysical time standard such as the Crab pulsar) was not available during these observations.

Some of the long timing observations contained a strong instrumental signal at 60 Hz and corresponding higher har-

[3] The same effect causes a sidereal day to be (1/365.25) d ≈ 4 minutes shorter than a solar day.

TABLE 2

OPTICAL PHOTOMETRY OF 4U 1626 − 67

Quantity	*U*	*B*	*V*	*R*	*I*
Source count rate (count s^{-1})	137(2)	122(2)	111(4)	177(3)	...
Pulsed count rate (count s^{-1}).....	7.9(3)	6.9(3)	7.0(5)	11.8(5)	25(2)
Sky count rate (count s^{-1})	168(2)	182(2)	317(4)	785(3)	5405(30)
Magnitude	17.50(29)	18.70(24)	18.68(15)	18.68(26)	...
Pulsed fraction	5.8(2)%	5.7(3)%	6.3(5)%	6.7(3)%	...
QPO fractional RMS strength.....	3.4%	2.7%	...	1.9%	...
QPO centroid frequency (Hz).....	0.048	0.049	...	0.049	...
QPO FWHM (Hz).....	0.013	0.012	...	0.009	...

monics in the 1 ms data (see Table 1). Whenever the 60 Hz signal was present, it was accompanied by a second strong signal at 1.75 Hz and its higher harmonics, and the two signals beat against each other. These high-frequency contaminants appeared intermittently in observations of several different targets. However, their presence did not affect any of the science analysis for 4U 1626−67, all of which was confined to pulse frequencies below 1 Hz.

3. RESULTS

Absolute photometry of 4U 1626−67 on May 26 yielded the following magnitude and colors: $V = 18.68(15)$, $U-B = -1.20(17)$, $B-V = 0.02(19)$, and $V-R = 0.00(21)$. The individual magnitudes are given in Table 2. The I-band sky background observation was too short to allow determination of a reliable source magnitude, but the presence of 7.66 s I-band pulsations, in phase with those in the bluer bands (see below), confirms that the source was detected in the I band as well. Assuming that the I-band pulsed fraction is also 6% (as in the other optical bands; see below), the source has $I = 17.8(3)$. Within the uncertainties, interstellar reddening can be neglected for this high-latitude source, since the total Galactic reddening in the direction of 4U 1626−67 is $E(B-V) \approx 0.09$ (Burstein & Heiles 1982). The UBV magnitudes reported here are virtually identical to those measured on 1977 June 12 by McClintock et al. (1977), and they agree to within 2 σ with those measured on 1977 August 17 by Grindlay (1978). However, the present R-band measurement is 1.8(4) mag brighter than previously reported by Grindlay (1978).

The observed time series were transformed to the solar system barycenter frame using the Jet Propulsion Laboratory DE-200 solar system ephemeris (Standish et al. 1992). Power spectra of the individual observations in all five bands showed strong 7.66 s pulsations, with a mean barycentric pulse frequency of 130.4398(7) mHz. This is consistent with the X-ray pulsation frequency measured at the midpoint of the CTIO observations by the BATSE all-sky monitor on the *Compton Gamma Ray Observatory* (Chakrabarty et al. 1997). To facilitate a study of the pulse shape and phase relationship of the optical pulsations at different wavelengths, a precise pulse phase ephemeris was derived from a subset of the BATSE observations (1995 May 9–June 11) contemporaneous with the CTIO observations. Based on these data, the barycentric X-ray pulse phase during the CTIO observations is well fitted by

$$\phi(t) = \phi_0 + \nu_0(t - t_0) + \tfrac{1}{2}\dot{\nu}(t - t_0)^2 , \qquad (1)$$

where $\phi_0 = 0.936758$, $\nu_0 = 0.1304376013765$ Hz, $\dot{\nu} = -6.32044 \times 10^{-13}$ Hz s^{-1}, $t_0 =$ 1995 May 27.5 TDB, and the pulse phase is defined relative to the intensity minimum of the fundamental harmonic of the 20–60 keV BATSE pulse profile.

The CTIO timing observations for each of the five filters were folded according to the timing model in equation (1). The resulting pulse profiles, along with the BATSE 20–60 keV pulse profile, are shown in Figure 1 relative to the BATSE pulse phase. The mean optical pulse and the BATSE hard X-ray pulse agree in phase to within 5% (i.e., a relative time delay of $\lesssim 0.4$ s), consistent with previous measurements (McClintock et al. 1980). Both the BATSE hard X-ray pulse and the optical pulse shapes have a dominant sinusoidal component, although the optical pulses clearly have additional harmonic content as well. The optical pulse shapes do not resemble any of the X-ray pulse shapes in the 2–13 keV range, all of which have an unusual and distinctive close double peak structure (Levine et al. 1988). Instead, the optical pulse shapes resemble the low-energy (1–2 keV) and high-energy (15–60 keV) pulse shapes. This is consistent with previous observations by McClintock et al. (1980), who concluded that the 1–2 keV X-rays were chiefly responsible for the reprocessed optical emission. The pulsed fraction, independent of wavelength, is approximately 6% (see Table 2), suggesting that the optical emission is dominated by X-ray reprocessing.

Figure 2 shows the Fourier power spectrum of a 2 hr U-band observation (run 15U). The spectrum has been rebinned into uniform logarithmic frequency intervals, the mean noise level due to Poisson counting statistics subtracted off, and the power level normalized relative to the double-sided mean source power (e.g., Miyamoto et al. 1994). In addition to the 130 mHz pulsation, a 0.048 Hz QPO was also detected. This feature was fit with a Lorentzian profile (e.g., Shibazaki & Lamb 1987),

$$P_{\rm QPO}(\nu) \propto \frac{(\Delta\nu/2)}{\pi} \frac{1}{(\Delta\nu/2)^2 + (\nu - \nu_{\rm QPO})^2} , \qquad (2)$$

where $\nu_{\rm QPO}$ is the centroid frequency of the QPO and $\Delta\nu$ is its full-width at half-maximum (FWHM). The fractional rms amplitude of the QPO was computed by integrating equation (2) over the FWHM of the feature and taking the square root, yielding 3.4% for this observation. The QPO is also detected in the B- and R-band observations. The best-fit parameters for the QPO features are included in Table 2. These measurements provide the first detection of an optical QPO from an X-ray pulsar. A similar feature is observed at X-ray wavelengths (Shinoda et al. 1990; Angelini et al. 1995; Chakrabarty et al. 1998). For comparison, the Fourier power spectrum of the 2–6 keV data from a 71 ks observation of 4U 1626−67 with the Proportional Counter Array on the *Rossi X-Ray Timing Explorer* (*RXTE*) is shown in Figure 3. This observation was made on 1996 February 11. The QPO is clearly visible in the X-ray data with an rms strength of 6%, along with several harmonics of the coherent 7.66 s pulsation. (The higher harmonics are very strong owing to the very sharp 2–6 keV X-ray pulse shape of 4U 1626−67.) The *RXTE* data will be discussed in further detail elsewhere (Chakrabarty et al. 1998).

To study the detailed structure of the optical timing properties close to the pulsation frequency, an overresolved power spectrum was constructed by computing the Fourier power $P_{k+\epsilon} = |H_{k+\epsilon}|^2$ at fractional bin intervals according to

$$H_{k+\epsilon} = \sum_{j=0}^{N-1} h_j e^{2\pi i j(k+\epsilon)/N} = \sum_{j=0}^{N-1} y_j^{(\epsilon)} e^{2\pi i jk/N} , \qquad (3)$$

with $0 < \epsilon < 1$, where $y_j^{(\epsilon)}$ is the original time series h_j multiplied by complex phase factors $e^{2\pi i j\epsilon/N}$. Note that while the N-shifted power spectrum bins $\{P_{k+\epsilon}\}$ are statistically independent of each other, they are *not* independent of the original power spectrum $\{P_k\}$ (although the covariances are easily computed; see, e.g., Jenkins & Watts 1968). Generalizing this process, one can construct an n-times overresolved power spectrum by interleaving the bins from the original power spectrum and $n-1$ frequency-shifted power spectra. Operationally, this is equivalent to padding the

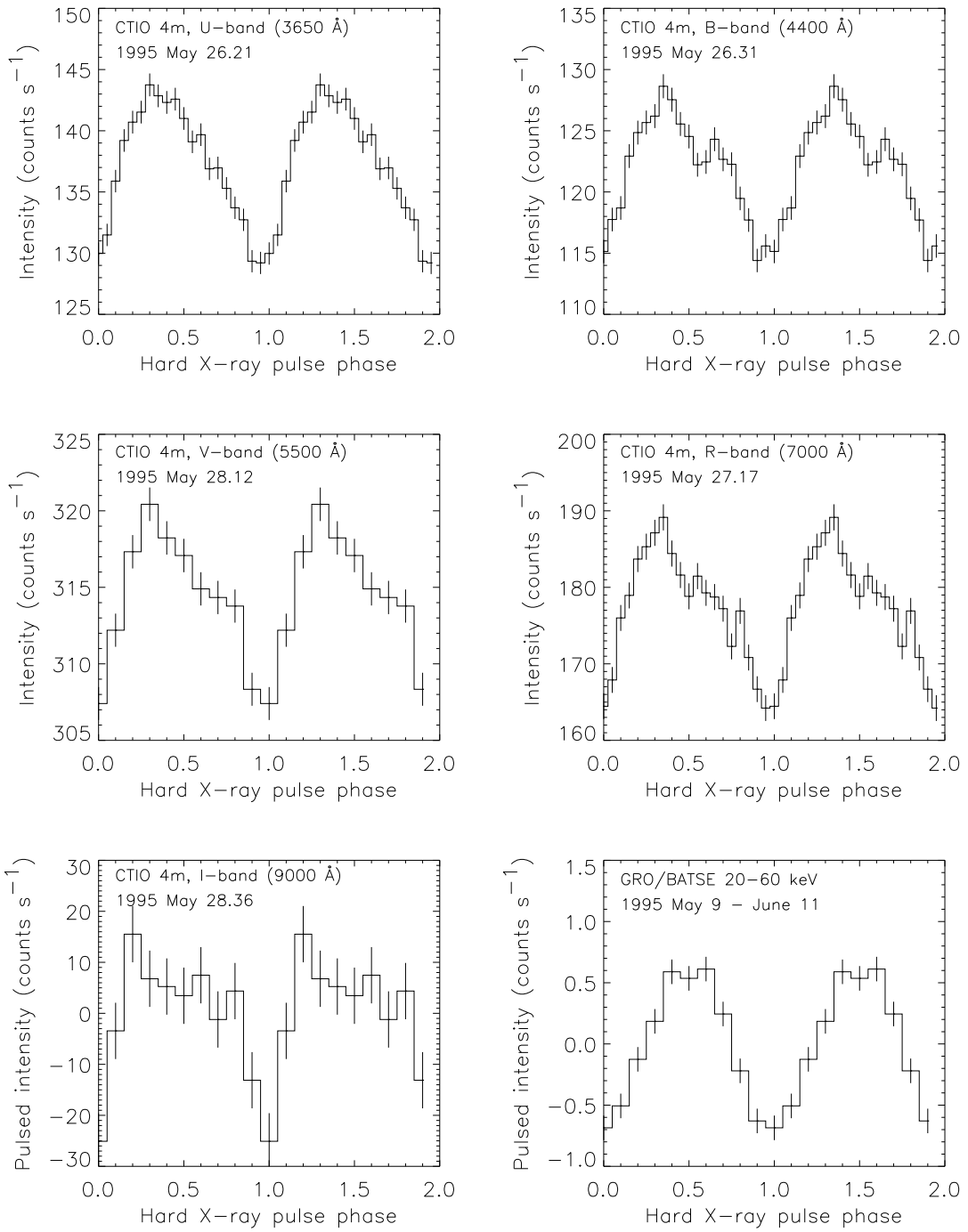

FIG. 1.—Optical pulse profiles as a function of wavelength for 4U 1626−67. Also shown is the 20–60 keV X-ray pulse profile, measured contemporaneously by BATSE. Two pulses are shown in each panel, and the pulse phase is plotted relative to the intensity minimum of the X-ray pulse. For the *I*-band optical and BATSE X-ray measurements, the intensity of the unpulsed (DC) component of the source emission was not measured.

original N-point zero-mean time series with $(n-1)N$ zeros and computing the power spectrum of the new nN-point padded time series. Use of an oversampled power spectrum gives more uniform frequency sensitivity at the expense of independent frequency bins, recovering Fourier phase information that is normally lost when constructing the power spectrum from the Fourier amplitudes.

Figure 4 shows a 5 times overresolved power spectrum of 4U 1626−67 in the immediate vicinity of the main pulsation. The power spectrum has been normalized relative to the mean noise power. To improve the signal-to-noise ratio, the power spectrum shown is the average of power spectra from three separate 1.8 hr observations (runs 15U, 17B, and 23R). In addition to the fundamental pulsation at 130.4398(37) mHz, several other features are present. In considering these features, it is important to recall that the peaks arising from periodic signals in a finite length power spectrum are always accompanied by sidelobes. This can be understood by considering a finite time series as the product of an infinite data stream and a rectangular (boxcar) observation window function (equal to unity during the observation and zero elsewhere). By the Fourier convolution

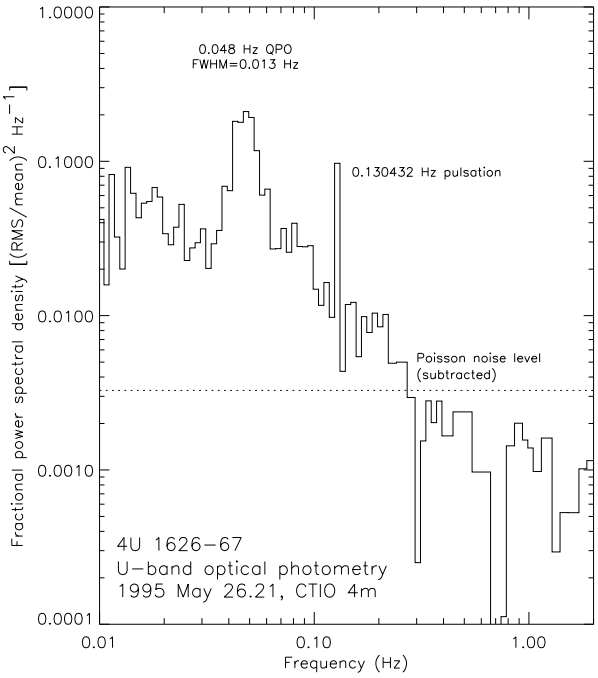

FIG. 2.—Fourier power density spectrum of a 2 hr U-band observation (run 15U) of 4U 1626−67 on 1995 May 26, normalized relative to the mean source power. The dotted line indicates the noise power level due to Poisson counting statistics, which has been subtracted off. A 0.048 Hz quasi-periodic oscillation with 4.9% fractional rms amplitude is clearly visible, as is the 7.66 s coherent pulsation due to the neutron star's rotation. An underlying $1/\nu$ spectrum is measured on timescales of $\lesssim 10$ s.

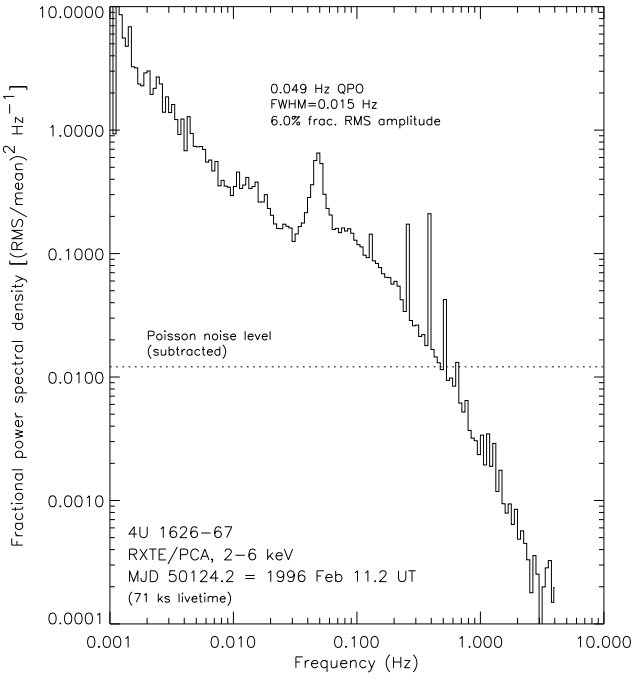

FIG. 3.—Fourier power density spectrum of a 71 ks 2–6 keV *RXTE*/PCA observation of 4U 1626−67 on 1996 Feb 11, normalized relative to the mean X-ray source power. The dotted line indicates the noise power level due to Poisson counting statistics, which has been subtracted off. Although this power spectrum cannot be directly compared to the optical power spectrum in Fig. 2 (since they were not acquired contemporaneously), the overall similarities are obvious and bolster the idea that the optical emission is dominated by rapid X-ray reprocessing. Several higher harmonics of the 0.1304 Hz coherent pulsation are observable from the highly nonsinusoidal X-ray pulse shape in the 2–6 keV band.

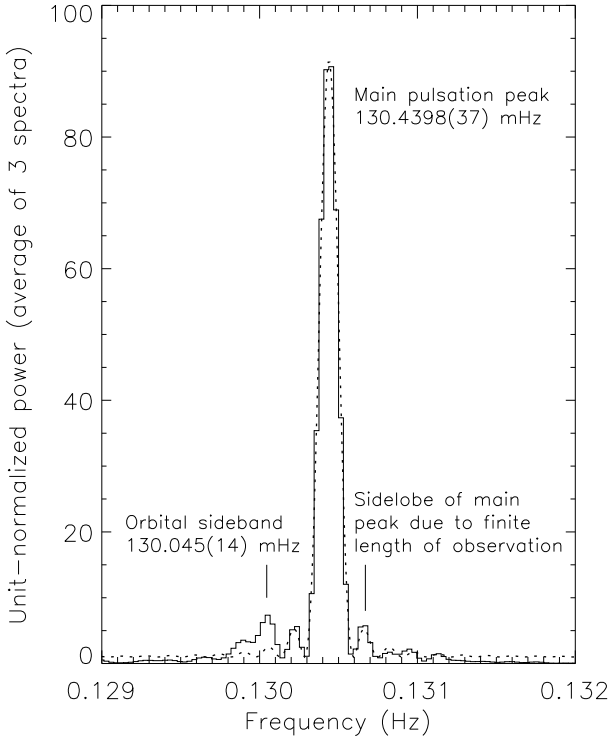

FIG. 4.—A 5 times overresolved Fourier power spectrum of 4U 1626−67 in the vicinity of the coherent 7.66 s pulsation, normalized relative to the local noise power. The solid line is the average of three separate power spectra of 1.8 hr observations. The dotted line is a model of the main pulsation's expected sidelobe resulting from the finite length of the power spectrum. This model can explain the symmetric sidelobes on either side of the main pulsation. A residual sideband downshifted 0.395(15) mHz from the main pulsation (25% relative amplitude) is also present, with a statistical significance of 4 σ. This frequency shift is consistent with a 2530 ± 100 s prograde binary orbit.

theorem, the Fourier transform of this product is equal to the convolution of the Fourier transforms of the infinite data stream and the observation window function (e.g., Press et al. 1992). Thus, the power at frequency ν due to a sinusoidal signal with frequency ν_0 in an ungapped observation of length T is

$$P(\nu) = P_0 \left[\frac{\sin \pi(\nu_0 - \nu)T}{\pi(\nu_0 - \nu)T} \right]^2 , \quad (4)$$

where P_0 is the power at the signal frequency. The dotted curve in Figure 4 shows the fit of this function to the data (with the expected mean noise level of unity added), assuming that $\nu_0 = 130.4398$ mHz corresponds to the main pulsation peak. The expected sidelobe structure almost exactly accounts for the two symmetric sidelobes on either side of the main peak.

However, after accounting for the expected sidelobe structure of the main pulsation, a residual power excess is clearly evident at $\nu = 130.045(14)$ mHz, downshifted 0.395(15) mHz from the main pulsation peak. This is consistent with the 0.4011(21) mHz shift for the lower sideband reported by Middleditch et al. (1981). The amplitude of the sideband relative to the main pulsation is 25% (compared to 20% measured by Middleditch et al. 1981), corresponding to a sideband pulsed fraction of 1.5%. To evaluate the statistical significance of this excess power, note that the powers in an average of three background-dominated

power spectra obey (within a constant scaling factor) a χ^2 distribution with 6 degrees of freedom. For a power spectrum normalized such that the mean noise power is unity, the probability of a noise fluctuation in a single bin exceeding a threshold power $P_{\rm thresh}$ is

$$\Pr\,(P > P_{\rm thresh}) = \tfrac{1}{16}\int_{6P_{\rm thresh}}^{\infty} t^2 e^{-t/2}\,dt\ . \qquad (5)$$

Thus, the observed excess power of 5.9 has a probability of 3.6×10^{-6} of being due to a random fluctuation, making it significant at the 4.6 σ level. Accounting for the fact that all bins in the range 0.129–0.132 Hz were searched reduces the statistical significance to 4.0 σ. It is especially striking to note that the frequency *shift* of the sideband agrees with that reported by Middleditch et al. (1981) despite the fact that the actual value of the main pulsation frequency (corresponding to the pulsar's spin) has changed from 130.26 mHz to 130.44 mHz in the 15 yr between the two observations (Chakrabarty et al. 1997). Our sideband detection strongly corroborates the 42 minute binary period reported by Middleditch et al. (1981). Unfortunately, the signal-to-noise ratio of this detection is insufficient to permit a more detailed investigation of the binary parameters.

4. DISCUSSION

4.1. *Multiwavelength Timing Signatures as Probes of LMXBs*

QPOs in accretion-powered pulsars are widely believed to arise from interactions between the pulsar magnetosphere and the inner edge of an accretion disk. In the beat frequency model (Alpar & Shaham 1985; Lamb et al. 1985), the QPO arises when inhomogeneous "clumps" of material at the inner edge of the disk are captured by the magnetosphere and accreted by the pulsar, producing a broad power spectral feature at the beat frequency $\nu_{\rm QPO} = \nu_{\rm K} - \nu_{\rm spin}$ between the Keplerian frequency at the inner disk edge and the pulsar spin frequency. (An alternative explanation, the Keplerian frequency model of van der Klis et al. 1987, predicts $\nu_{\rm QPO} = \nu_{\rm K}$. However, it can only explain QPOs where $\nu_{\rm QPO} > \nu_{\rm spin}$, and thus is not applicable to 4U 1626−67.) Thus, the 0.048 Hz X-ray QPO in 4U 1626−67 bolsters the premise that this is a disk-fed binary.

The discovery of an optical QPO at the same frequency shows that a significant fraction of the optical luminosity from the binary simply mirrors the X-ray emission, and must therefore result from X-ray reprocessing. As noted by Middleditch et al. (1981), the existence of two distinct, persistent, coherent optical pulsation frequencies suggests that the reprocessing occurs in two separate sites, most likely the surface of the mass donor and the accretion disk. Simultaneous X-ray and optical timing of these pulsations and the QPO may therefore provide a powerful probe of the geometry of the binary and the physics of the accretion disk (e.g., Arons & King 1993).

Unfortunately, the BATSE hard X-ray measurements acquired simultaneously with the optical observations require $\gtrsim 1$ day to detect the X-ray pulsations, making them useless for a correlating study on short timescales. However, more sensitive X-ray timing missions (e.g., *RXTE*) are well suited to such a task if the observations can be coordinated with ground-based optical observations. A comparison of Figures 2 and 3 gives the flavor of the kind of data sets that can be directly compared if measured simultaneously. Ultraviolet timing observations with the *Hubble Space Telescope* may also provide an important probe, as the reprocessing in the disk should be more efficient at these wavelengths than in the optical (Arons & King 1993; Anderson et al. 1997). More generally, time-resolved ultraviolet/optical/infrared photometry may provide an important test for candidate multiwavelength counterparts in time-variable LMXBs for which the companion remains unidentified.

4.2. *Nature of the Mass Donor and the Mass Transfer*

While X-ray binaries and cataclysmic variables with a hydrogen-rich mass donor cannot reach orbital periods $P_{\rm orb} \lesssim 80$ minutes (Paczyński & Sienkiewicz 1981), those with a hydrogen-depleted mass donor can evolve to extraordinarily short ($P_{\rm orb} \sim 10$ minutes) orbital periods while maintaining high mass transfer rates (Nelson, Rappaport, & Joss 1986). A few such systems are known, including the six AM CVn cataclysmic variables (see Warner 1995) and the X-ray bursters 4U 1820−30 ($P_{\rm orb} =$ 11 minutes) and 4U 1916−05 ($P_{\rm orb} = 50$ minutes). The recently reported 20.6 minute ultraviolet modulation in the X-ray burster 4U 1850−087 is probably due to the same phenomenon (Homer et al. 1996). With a 42 minute binary period, 4U 1626−67 is clearly also a member of this class (Levine et al. 1988).

In addition to the inferred 42 minute binary period, there are several other constraints on scenarios for the mass donor in 4U 1626−67. The stringent X-ray timing limit ($a_{\rm X} \sin i < 8$ lt-ms; Levine et al. 1988; Shinoda et al. 1990) on the projected radius of the pulsar orbit implies

$$\sin i < 7.8 \times 10^{-3} q^{-1}(1+q)^{2/3} M_{1.4}^{-1/3} P_{42}^{-2/3}\ , \qquad (6)$$

where $q = M_*/M_{\rm X}$ is the mass ratio, M_* is the companion mass, $M_{1.4}$ is the neutron star mass $M_{\rm X}$ in units of 1.4 $M_\odot$, and P_{42} is the binary period in units of 42 minutes. The a priori probability of observing a system within the inclination limit $i < i_{\rm max}$ is given by $(1 - \cos i_{\rm max})$.

A second constraint is the assumption that the mass transfer in an ultracompact binary is driven by angular momentum losses via gravitational radiation (e.g., Levine et al. 1988). The resulting mass transfer rate will be (e.g., Verbunt & van den Heuvel 1995 and references therein)

$$\dot{M} = 8.3 \times 10^{-8} M_{1.4}^{8/3} q^2 (1+q)^{-1/3} \times \left(\frac{5}{6} + \frac{n}{2} - q\right)^{-1} M_\odot\ {\rm yr}^{-1}\ , \qquad (7)$$

where n is the power-law exponent in the companion's mass-radius relation ($R_* \propto M_*^n$), and conservative mass transfer via Roche lobe overflow has been assumed. Since the bolometric X-ray flux from 4U 1626−67 has been measured ($F_{\rm X} = 2.4 \times 10^{-9}$ erg cm^{-2} s^{-1} in the 0.5–60 keV band; Pravdo et al. 1979), this also constrains the source distance and X-ray luminosity $L_{\rm X} = GM_{\rm X}\dot{M}/R_{\rm X} = 4\pi D^2 F_{\rm X}$, where $R_{\rm X} \approx 10$ km is the neutron star radius and D is the distance to the source.

Another constraint is a lower limit on $\dot{M}$ from the observed spin history of the pulsar (Chakrabarty et al. 1997). If the pulsar is spinning up, then the maximum possible accretion torque on the neutron star will occur when the magnetospheric radius r_m (where the magnetic energy

density is comparable to the kinetic energy density of the accreting matter) is close to the corotation radius r_{co} (where the magnetic field lines move with the local disk velocity). This limit may be written as $N \lesssim \dot{M}(GM_x r_{co})^{1/2}$, where $r_{co} = (GM_x/4\pi^2\nu^2)^{1/3}$ for a Keplerian disk. However, the torque on the neutron star can be rewritten as $N = 2\pi I_x \dot{\nu}$, where $I_x \approx (2/5)M_x R_x^2$ is the pulsar's moment of inertia (Ravenhall & Pethick 1994) and $\dot{\nu}$ is the spin frequency derivative—a directly measurable quantity. Noting that $\dot{\nu} = 8.5 \times 10^{-13}$ Hz s^{-1} was measured during the spin-up of 4U 1626−67, Chakrabarty et al. (1997) thus inferred that $\dot{M} \gtrsim 2 \times 10^{-10}\ M_\odot$ yr^{-1}.

Given the measured X-ray flux, the $\dot{M}$ limit requires $D \gtrsim 3$ kpc. In view of the source's high Galactic latitude ($b = -13°$), the resulting distance out of the plane is also a consideration when contemplating mass donors. However, this need not be a strong consideration, since it is plausible that neutron star LMXBs may have high velocities due to a supernova "kick," leading to a considerable distance from the plane over the long X-ray lifetime of the source. Indeed, the high-latitude ($b = 38°$) LMXB pulsar Her X-1/HZ Her is 6.6 ± 0.4 kpc distant, over 4 kpc out of the plane (Reynolds et al. 1997).

The possible types of Roche lobe–filling mass donors for 4U 1626−67 have been discussed previously by Levine et al. (1988) and Verbunt, Wijers, & Burm (1990). I review and update those discussions here. There are three possible types of Roche lobe–filling donors for a 42 minute neutron star binary. The first possibility is a 0.02 $M_\odot$ helium or carbon-oxygen white dwarf. From equation (6), the binary inclination for this case must be $i \lesssim 33°$, with an a priori observation probability of 16%. The mass-radius relation for such a star is $R_* \propto M_*^{-1/3}$ (Shapiro & Teukolsky 1983), so the mass transfer rate from equation (7) is $3 \times 10^{-11}\ M_\odot$ yr^{-1}. This corresponds to a distance of about 1 kpc. Although this case has the most favorable inclination constraint of the Roche lobe–filling options (because of the extremely small M_*), the mass transfer rate driven by gravitational radiation alone is an order of magnitude below the minimum mass accretion rate inferred by Chakrabarty et al. (1997).

The second Roche lobe–filling possibility is a 0.08 $M_\odot$ hydrogen-depleted star that is not fully degenerate, with $i \lesssim 8°$ and an a priori probability of 1%. Assuming $R_* \propto M_*$, equation (7) gives $\dot{M} = 2 \times 10^{-10}\ M_\odot$ yr^{-1}, corresponding to a distance of 3 kpc. These are identical to the lower limits on $\dot{M}$ and D inferred from the pulsar spin-up measurements, and thus are just consistent with the observations. Finally, a 0.6 $M_\odot$ Roche lobe–filling helium-burning star is also a possible donor for a 42 minute neutron star binary. However, the small allowed inclination range ($i < 1.^\circ3$) has an a priori observation probability of only 0.03%, and the expected mass transfer rate ($\dot{M} = 3 \times 10^{-8}\ M_\odot$ yr^{-1}; Savonije, de Kool, & van den Heuvel 1986) would require an unphysically large distance (36 kpc) to be consistent with the observed X-ray flux.

Angelini et al. (1995) have proposed an alternative to a Roche lobe–filling donor. These authors detected an unusually strong complex of neon emission lines in the X-ray spectrum of 4U 1626−67. Since neon is a product of helium burning, Angelini et al. (1995) suggest that the mass donor is a helium-burning star that underfills its Roche lobe, transferring matter to the neutron star via a radiatively driven wind. This possibility is of particular interest given the suggestion that the current spin-down of the pulsar is due to accretion from a retrograde disk (Nelson et al. 1997), since formation of such a disk is much more plausible for wind accretion than for Roche lobe overflow.

However, the wind from a low-mass helium-burning star would not provide a high enough mass transfer rate to be consistent with the X-ray data, as is now shown. A mass of $\gtrsim 0.3\ M_\odot$ is required for core helium burning (Kippenhahn & Weigert 1990). A 0.3 $M_\odot$ helium-burning donor would fill about 25% of its Roche lobe (Eggleton 1983) and would have $R_* = 0.07\ R_\odot$ and an effective temperature $T_* = 2 \times 10^4$ K (Savonije et al. 1986), yielding a blackbody spectrum consistent with or fainter than the optical photometry for distances $\gtrsim 4$ kpc. More generally, helium-burning donors with $M_* \lesssim 0.6\ M_\odot$ would underfill the Roche lobe and be consistent with or fainter than the optical measurements for somewhat larger distances, with $R_* \lesssim 0.14\ R_\odot$ and $T_* \lesssim 4 \times 10^4$ K. Assuming a radiatively driven wind similar to that observed in other hot stars, the wind mass loss rate with these parameters would be $-\dot{M}_w \lesssim 10^{-11}\ M_\odot$ yr^{-1} (Abbott 1982). Especially in light of the poor accretion efficiency expected for a wind-fed system (<0.01; e.g., Frank, King, & Raine 1992), this is much too small to be consistent with the inferred accretion rate, $\dot{M} \gtrsim 2 \times 10^{-10}\ M_\odot$ yr^{-1}. Similar considerations seem to rule out any plausible donor transferring matter via a conventional radiatively driven wind. On the other hand, a self-excited wind arising from X-ray heating of the mass donor might be a significant contributor to the mass transfer rate, whether or not the donor fills its Roche lobe (see Tavani & London 1993 and references therein).

4.3. *Origin of the Optical Emission*

It is instructive to consider whether a stellar spectrum can explain the optical photometry. The data can in fact be well fitted by a single-temperature (stellar) blackbody spectrum,

$$F_{\nu^*} = \frac{R_*^2}{D^2} \frac{2\pi h\nu^3/c^2}{\exp\,(h\nu/kT_*) - 1}\,, \tag{8}$$

where F_{ν^*} is the flux density from the star per unit frequency ν, R_* is the stellar radius, D is the source distance, $h = 6.6 \times 10^{-27}$ ergs s is Planck's constant, c is the velocity of light, $k = 1.38 \times 10^{-16}$ ergs K^{-1} is Boltzmann's constant, and T_* is the effective temperature of the star. The best-fit parameters are $T_* = 1.8 \times 10^4$ K and $R_*/D = 7.3 \times 10^{-13}$, so that $D = 32(R_*/R_\odot)$ kpc. A hydrogen-burning star with the correct temperature (a main-sequence or supergiant B star) is obviously excluded both by the absurd ($D \gtrsim 100$ kpc) distance required and by the infinitesimal a priori probability for the necessary binary inclination. A 0.3 $M_\odot$ helium-burning star with $D \approx 2$ kpc would have the correct temperature and flux. However, as noted above, it would severely underfill its Roche lobe and so probably could not transfer sufficient mass to the pulsar to explain the observed X-ray flux. In addition, the implied binary inclination for a 42 minute orbit has an a priori probability of $<0.1\%$.

However, assuming a typical white dwarf mass-radius relation, $(R_*/R_\odot) \approx 0.01(M_*/M_\odot)^{-1/3}$ (Shapiro & Teukolsky 1983), we find $D \approx 1$ kpc for a 0.02 $M_\odot$ white dwarf. As noted above, such a star would just fill its Roche lobe, and the expected mass transfer rate would be consistent with the observed X-ray flux. For such a close binary, X-ray heating would certainly dominate the intrinsic luminosity of

the degenerate dwarf. Assuming isotropic X-ray emission, we have

$$T_* \approx \left[\frac{1}{4}\frac{R_*^2}{a^2}\frac{L_X(1-\eta_*)}{\pi\sigma R_*^2}\right]^{1/4} = \left[\frac{L_X(1-\eta_*)}{4\pi\sigma a^2}\right]^{1/4} = 2.1\times 10^4 P_{42}^{-1/3} D_{kpc}^{1/2}(1+q)^{-1/6}(1-\eta_*)^{1/4}\ \mathrm{K}\ , \quad (9)$$

where a is the binary separation, η_* is the X-ray albedo of the white dwarf, and $F_X = 2.4\times 10^{-9}$ ergs cm^{-1} s^{-1} has been used for the X-ray flux (Pravdo et al. 1979). Thus, X-ray heating of a low-mass white dwarf would naively seem to provide a plausible model for the observed optical emission.

Unfortunately, this is an unrealistic model. The 0.04 Hz QPO detected in the X-ray and optical data underscores the presence of an accretion disk (e.g., van der Klis 1995) that must contribute significant optical luminosity. The flux from a geometrically thin, optically thick disk can be written as

$$F_{vd} = \frac{4\pi h\nu^3\cos i}{c^2 D^2}\int_{r_{in}}^{r_{out}}\frac{r\,dr}{\exp\left[h\nu/kT(r)\right]-1}\ , \quad (10)$$

where $T(r)$ is the disk's surface temperature as a function of midplane radius r. Given the X-ray timing limits, it is clear that $\cos i \approx 1$. The outer disk may be assumed to cut off sharply at the tidal radius of the neutron star ($\approx 0.9 R_{Roche}$; Frank et al. 1992), corresponding to $r_{out} \approx 2\times 10^{10}$ cm for 4U 1626−67. The inner accretion disk should be disrupted by the pulsar's magnetosphere at roughly the neutron star's corotation radius, $r_{in} \approx r_{co} = 6.5\times 10^8$ cm for a Keplerian disk. (Strictly speaking, r_{co} is an upper limit on r_{in}, but the calculation is not sensitive to this quantity since most of the disk's optical emission comes from its outer parts.) For an X-ray heated disk, the disk may be considered to consist of up to three distinct regions: an innermost region powered primarily by internal viscous dissipation, a middle region of "shallow" X-ray heating, and an outer region of "deep" X-ray heating (e.g., Cunningham 1976; Arons & King 1993). Let us consider each of these regions in turn.

The standard temperature profile for an unirradiated thin accretion disk is set by internal viscous dissipation (Shakura & Sunyaev 1973; Frank et al. 1992)

$$T_0 = \left(\frac{3GM_x\dot{M}}{8\pi\sigma r^3}\right)^{1/4} = 7100 M_{1.4}^{1/4}\dot{M}_{-10}^{1/4} r_{10}^{-3/4}\ \mathrm{K}\ , \quad (11)$$

where $\sigma = 5.67\times 10^{-5}$ ergs cm^{-2} K^{-4} s^{-1} is the Stefan-Boltzmann constant, $M_{1.4}$ is the neutron star mass in units of 1.4 $M_\odot$, $\dot{M}_{-10}$ is the mass accretion rate in units of 10^{-10} $M_\odot$ yr^{-1}, and r_{10} is the midplane radius in units of 10^{10} cm. At sufficiently small radii, this internal heating will dominate over X-ray heating in setting the disk temperature. Beyond a critical radius, however, X-ray heating of the disk surface will modify the temperature profile according to

$$T_{irr} = (T_0^4 + T_X^4)^{1/4}\ . \quad (12)$$

Assuming that the disk is irradiated by a central X-ray point source, then we can write T_X as

$$T_X = \left[\frac{L_X(1-\eta_d)}{4\pi\sigma r^2}\cos\psi\right]^{1/4} \approx \left[\frac{L_X(1-\eta_d)}{4\pi\sigma r^2}\left(\frac{dH}{dr}-\frac{H}{r}\right)\right]^{1/4}\ , \quad (13)$$

where η_d is the X-ray albedo of the disk, ψ is the angle between the normal to the disk surface and the vector from the neutron star, and H is the disk's scale height. Thus, we see that the temperature profile from X-ray heating is sensitive to the functional form of $H(r)$ through the approximation for $\cos\psi$ (which assumes $H \ll r$).

In the shallow X-ray heating region, the surface temperature profile is set by X-ray heating, but the *central* temperature of the disk is still set by internal viscous dissipation. Thus, the disk thickness has the usual value for a standard unirradiated thin disk (Shakura & Sunyaev 1973; Frank et al. 1992),

$$H = 1.2\times 10^8 \alpha^{-1/10}\mu^{-3/8} M_{1.4}^{-3/8}\dot{M}_{-10}^{3/20} r_{10}^{9/8}\ \mathrm{cm}\ , \quad (14)$$

where α is an order unity dimensionless parametrization of the kinematic viscosity $\nu_{visc} = \alpha c_s H$, c_s is the isothermal sound speed, and μ is the mean molecular weight in units of the hydrogen atomic mass. (Note that $\mu = 1$ for neutral hydrogen, 1/2 for ionized hydrogen, 4 for neutral helium, 2 for singly ionized helium, and 4/3 for doubly ionized helium.) We thus find

$$T_X = 1.2\times 10^4 \alpha^{-1/40}\mu^{-3/32}(1-\eta_d)^{1/4} M_{1.4}^{5/32} \times \dot{M}_{-10}^{23/80} r_{10}^{-15/32}\ \mathrm{K}\ . \quad (15)$$

Shallow X-ray heating will dominate internal viscous heating in setting the disk surface temperature when $T_X \gtrsim T_0$, which occurs at radii exceeding roughly 10^9 cm.

If $T_X^4 \gtrsim \tau T_0^4$, then X-ray heating will also dominate internal heating in setting the *central* temperature of the disk (Lyutyi & Sunyaev 1976; Spruit 1995). Here, τ is the disk's optical depth, given by $\tau = 34\alpha^{-4/5}\mu^{1/4}\dot{M}_{-10}^{1/5}$ for a standard α-disk (Frank et al. 1992). In this region of deep X-ray heating, the vertical structure of the disk will not obey the $H \propto r^{9/8}$ relationship in equation (14), but will instead follow a $H \propto r^{9/7}$ power law (e.g., Cunningham 1976; Vrtilek et al. 1990; Arons & King 1993). However, deep X-ray heating will dominate over shallow heating only for radii exceeding roughly 2×10^{10} cm. In a binary as compact as 4U 1626−67, the disk will terminate before deep heating becomes dominant, so that a combination of internal viscous heating and shallow X-ray heating (eqs. [12], [11], and [15]) should be valid over the entire disk.

Accounting for the presence of an X-ray–heated accretion disk, it is clear that the model of an X-ray–heated low-mass white dwarf at a distance of 1 kpc is untenable for 4U 1626−67, since the expected optical emission from the disk would be considerably brighter than the measured fluxes. Instead, it is more appropriate to consider the opposite case, in which the disk provides most of the optical luminosity, by fitting equations (10) and (12), along with equations (11) and (15), to the measured optical photometry. The free parameters for the fit are D (or, equivalently, L_X) and η_d. As is evident from Figure 5, the X-ray heated disk model can easily fit the data.

However, as shown in Figure 6, the optical data do not provide a strong joint constraint on D and η_d. Ultraviolet observations will eventually provide a much stronger constraint, since the UV spectrum from an X-ray–heated disk is much more sensitive to the values of L_X and η_d. In the absence of ultraviolet observations, it should be noted that de Jong, van Paradijs, & Augusteijn (1996) have concluded that LMXB accretion disks have a very high effective X-ray albedo ($\eta_d \gtrsim 0.9$), based on observations of 4U 1254−69,

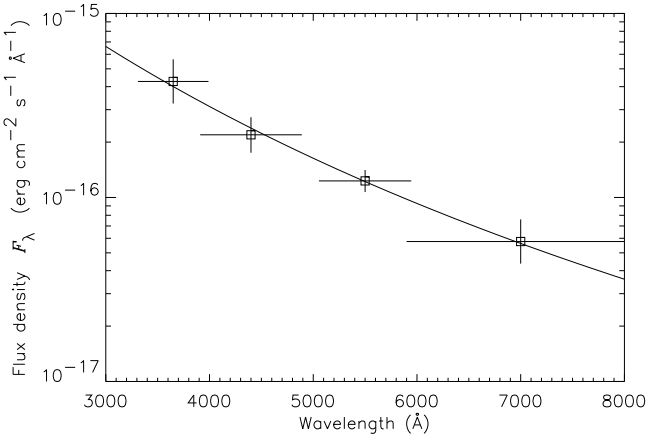

FIG. 5.—Optical (*UBVRI*) photometry of 4U 1626−67 on 1995 May 26. The solid curve indicates a typical X-ray–heated disk solution. The particular solution shown assumes $\eta_d = 0.95$, $D = 8.5$ kpc, $r_{\rm in} = 6.5 \times 10^8$ cm, and $r_{\rm out} = 2 \times 10^{10}$ cm. However, a range of values for η_d and D provide a good fit to the data (see Fig. 6).

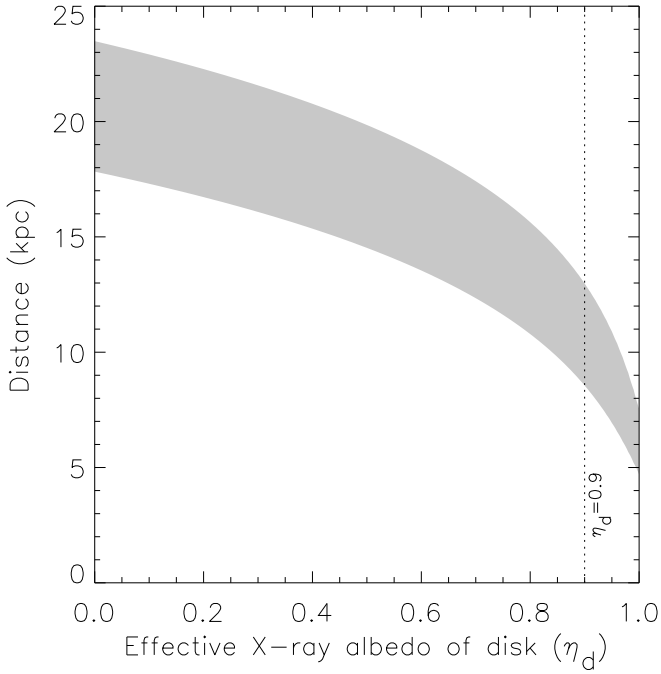

FIG. 6.—Distance to 4U 1626−67 as a function of effective X-ray albedo of the disk, assuming that all the optical flux is due to an X-ray–heated accretion disk with $r_{\rm in} = 6.5 \times 10^8$ cm, and $r_{\rm out} = 2 \times 10^{10}$ cm. The shaded region is consistent with the optical photometric data at a 95% confidence level. Based on observations of other LMXBs, de Jong et al. (1996) conclude that $\eta_d \gtrsim 0.9$. If this is correct, then the solutions allowed by the data must lie in the shaded region to the right of the vertical dotted line.

4U 1755−33, and Sco X-1. If this is the case in 4U 1626−67, then the optical data constrain the distance to $5 \lesssim D \lesssim 13$ kpc (95% confidence), corresponding to an X-ray luminosity of $7 \times 10^{36} \lesssim L_{\rm X} \lesssim 5 \times 10^{37}$ erg s^{-1}.

I am grateful to John Grunsfeld for first interesting me in this project. It is a pleasure to thank Andy Layden, Ramon Galvez, Patricio Ugarte, and the CTIO staff for their assistance and excellent support. I gratefully acknowledge a generous thesis observing travel award from CTIO. I thank Lars Bildsten, Josh Grindlay, Arlo Landolt, Al Levine, Rob Nelson, Tom Prince, and Brian Vaughan for useful discussions. This work was funded in part by a NASA GSRP Graduate Fellowship under grant NGT-51184, and by a NASA Compton Postdoctoral Fellowship under grant NAG 5-3109.

REFERENCES

Abbott, D. C. 1982, ApJ, 259, 282
Alpar, M. A., & Shaham, J. 1985, Nature, 316, 239
Anderson, S. F., Margon, B., Deutsch, E. W., Downes, R. A., & Allen, R. G. 1997, ApJ, 482, L69
Angelini, L., White, N. E., Nagase, F., Kallman, T. R., Yoshida, A., Takeshima, T., Becker, C. M., & Paerels, F. 1995, ApJ, 449, L41
Arons, J., & King, I. R. 1996, ApJ, 413, L121
Beehler, R. E., & Lombardi, M. A. 1990, NIST Time and Frequency Services (Boulder: National Inst. Standards and Technol.)
Burstein, D., & Heiles, C. 1982, AJ, 87, 1165
Chakrabarty, D. 1996, Ph.D. thesis, California Inst. Technology
Chakrabarty, D., et al. 1997, ApJ, 474, 414
———. 1998, in preparation
Chester, T. J. 1979, ApJ, 227, 569
Cunningham, C. 1976, ApJ, 208, 534
Davidsen, A., Henry, J. P., Middleditch, J., & Smith, H. E. 1972, ApJ, 177, L97
de Jong, J. A., van Paradijs, J., & Augusteijn, T. 1996, A&A, 314, 484
Eggleton, P. P. 1983, ApJ, 268, 368
Frank, J., King, A., & Raine, D. 1992, Accretion Power in Astrophysics (2nd ed.; Cambridge: Cambridge Univ. Press)
Graham, J. A. 1982, PASP, 94, 244
Grindlay, J. E. 1978, ApJ, 225, 1001
Homer, L., Charles, P. A., Naylor, T., van Paradijs, J., Aurière, M., & Koch-Miramond, L. 1996, MNRAS, 282, L37
Ilovaisky, S. A., Motch, C., & Chevalier, C. 1978, A&A, 70, L19
Imamura, J. N., Kristian, J., Middleditch, J., & Steiman-Cameron, T. Y. 1990, ApJ, 365, 312
Jablonski, F. J., Pereira, M. G., Braga, J., & Gneiding, C. D. 1997, ApJ, 482, L171
Jenkins, G. M., & Watts, D. G. 1968, Spectral Analysis and Its Applications (San Francisco: Holden-Day)
Joss, P. C., Avni, Y., & Rappaport, S. 1978, ApJ, 221, 645
Kippenhahn, R., & Weigert, A. 1990, Stellar Structure and Evolution (Berlin: Springer)
Lamb, F. K., Shibazaki, N., Alpar, M. A., & Shaham, J. 1985, Nature, 317, 681
Lewin, W. H. G., van Paradijs, J., & Taam, R. E. 1993, Space Sci. Rev., 62, 223
Levine, A., Ma, C. P., McClintock, J., Rappaport, S., van der Klis, M., & Verbunt, F. 1988, ApJ, 327, 732
Li, F. K., Joss, P. C., McClintock, J. E., Rappaport, S., & Wright, E. L. 1980, ApJ, 240, 628
Lyutyi, V. M., & Sunyaev, R. A. 1976, Sov. Astron., 20, 290
McClintock, J. E., Canizares, C. R., Bradt, H. V., Doxsey, R. E., Jernigan, J. G., & Hiltner, W. A. 1977, Nature, 270, 320
McClintock, J. E., Canizares, C. R., Li, F. K., & Grindlay, J. E. 1980, ApJ, 235, L81
Middleditch, J., Mason, K. O., Nelson, J. E., & White, N. E. 1981, ApJ, 244, 1001
Middleditch, J., & Nelson, J. 1976, ApJ, 208, 567
Miyamoto, S., Kitamoto, S., Iga, S., Hayashida, K., & Terada, K. 1994, ApJ, 435, 398
Motch, C., Ilovaisky, S. A., & Chevalier, C. 1982, A&A, 109, L1
Motch, C., Ricketts, M. J., Page, C. G., Ilovaisky, S. A., & Chevalier, C. 1983, A&A, 119, 171
Nelson, L. A., Rappaport, S. A., & Joss, P. C. 1986, ApJ, 304, 231
Nelson, R. W., et al. 1997, ApJ, 488, L117
Paczyński, B., & Sienkiewicz, R. 1981, ApJ, 248, L27
Pravdo, S. H., et al. 1979, ApJ, 231, 912
Press, W. H., Teukolsky, S. A., Vetterling, W. T., & Flannery, B. P. 1992, Numerical Recipes in C: The Art of Scientific Computing (2d ed.; Cambridge: Cambridge Univ. Press)
Ravenhall, D. G., & Pethick, C. J. 1994, ApJ, 424, 846
Reynolds, A. P., Quaintrell, H., Still, M. D., Roche, P. D., Chakrabarty, D., & Levine, S. E. 1997, MNRAS, 288, 43
Savonije, G. J., de Kool, M., & van den Heuvel, E. P. J. 1986, A&A, 155, 51
Shakura, N. I., & Sunyaev, R. A. 1973, A&A, 24, 337
Shapiro, S. L., & Teukolsky, S. A. 1983, Black Holes, White Dwarfs, and Neutron Stars (New York: Wiley)

Shibazaki, N., & Lamb, F. K. 1987, ApJ, 318, 767
Shinoda, K., Kii, T., Mitsuda, K., Nagase, F., Tanaka, Y., Makishima, K., & Shibazaki, N. 1990, PASJ, 42, L27
Spruit, H. C. 1995, in The Lives of the Neutron Stars, ed. M. A. Alpar, U. Kiziloglu, & J. van Paradijs (Dordrecht: Kluwer), 355
Standish, E. M., Newhall, X. X., Williams, J. G., & Yeomans, D. K. 1992, in Explanatory Supplement to the Astronomical Almanac, ed. P. K. Seidelmann (Mill Valley: University Science), 279
Tavani, M., & London, R. 1993, ApJ, 410, 281
van der Klis, M. 1995, in X-Ray Binaries, ed. W. H. G. Lewin, J. van Paradijs, & E. P. J. van den Heuvel (Cambridge: Cambridge Univ. Press), 252
van der Klis, M., Jansen, F., van Paradijs, J., Lewin, W. H. G., Sztajno, M., & Trümper, J. 1987, ApJ, 313, L19
van Paradijs, J., & McClintock, J. E. 1995, in X-Ray Binaries, ed. W. H. G. Lewin, J. van Paradijs, & E. P. J. van den Heuvel (Cambridge: Cambridge Univ. Press), 58
Verbunt, F., & van den Heuvel, E. P. J. 1995, in X-Ray Binaries, ed. W. H. G. Lewin, J. van Paradijs, & E. P. J. van den Heuvel (Cambridge: Cambridge Univ. Press), 457
Verbunt, F., Wijers, R. A. M. J., & Burm, H. M. G. 1990, A&A, 234, 195
Vrtilek, S. D., Raymond, J. C., Garcia, M. R., Verbunt, F., & Hasinger, G. 1990, A&A, 235, 162
Warner, B. 1995, Ap&SS, 225, 249